Improving the High Order Spectral Volume Formulation Using a Diffusion Regulator

Ravi Kannan[1],[*] and Zhijian Wang[2]

[1] *CFD Research Corporation, 215 Wynn Drive, Huntsville, AL 35805, USA.*
[2] *Iowa State University, Howe Hall, Ames, IA 50011, USA.*

Abstract. The concept of diffusion regulation (DR) was originally proposed by Jaisankar for traditional second order finite volume Euler solvers. This was used to decrease the inherent dissipation associated with using approximate Riemann solvers. In this paper, the above concept is extended to the high order spectral volume (SV) method. The DR formulation was used in conjunction with the Rusanov flux to handle the inviscid flux terms. Numerical experiments were conducted to compare and contrast the original and the DR formulations. These experiments demonstrated (i) retention of high order accuracy for the new formulation, (ii) higher fidelity of the DR formulation, when compared to the original scheme for all orders and (iii) straightforward extension to Navier Stokes equations, since the DR does not interfere with the discretization of the viscous fluxes. In general, the 2D numerical results are very promising and indicate that the approach has a great potential for 3D flow problems.

AMS subject classifications: 65

Key words: Diffusion regulation, spectral volume, high-order, Rusanov flux, Navier Stokes equations.

1 Introduction

The spectral volume (SV) method is a high order method, originally developed by Wang, Liu and their collaborators for hyperbolic conservation laws on unstructured grids [18, 26–30]. The spectral volume method can be viewed as an extension of the Godunov method to higher order by adding more degrees-of-freedom (DOFs) in the form of subcells in each cell (simplex). The simplex is referred to as a spectral volume and the subcells are referred to as control volumes (CV). All the spectral volumes are partitioned in a geometrically similar manner in a simplex, and thus a single reconstruction is obtained. As

---

[*]Corresponding author. *Email addresses:* `sunshekar@gmail.com` (R. Kannan), `zjw@iastate.edu` (Z. J. Wang)

in the finite volume method, the unknowns (or DOFs) are the subcell-averaged solutions. A finite volume procedure is employed to update the DOFs.

The spectral volume method was successfully implemented for 2D Euler [29] and 3D Maxwell equations [18]. Recently Sun et al. [24] implemented the SV method for the Navier Stokes equations using the LDG [6] approach to discretize the viscous fluxes. Kannan and Wang [11] conducted some Fourier analysis for a variety of viscous flux formulations. Kannan implemented the spectral volume method for the Navier Stokes equations using the LDG2 (which is an improvised variant of the LDG approach) [12] and DDG approaches [13]. Even more recently, Kannan extended the spectral volume method to solve the moment models in semiconductor device simulations [8–10]. Other developments include the formulation of a new boundary condition [14] and the implementation for elastohydrodynamic problems [15]. These past studies have demonstrated the efficacy of the spectral volume method for a wide range of engineering applications, and have established its robustness.

In spite of all the above developments, the handling of the inviscid fluxes has undergone minimal changes since the inception of the spectral volume method. Till date, almost all of spectral volume implementations use the Rusanov or the Roe formulation as the approximate Riemann flux. These fluxes utilize an artificial dissipation term (or a matrix) as a straight-forward addition to the averaged flux (central discretization). This simplistic flux evaluation procedure has yielded acceptable results.

In this paper, we borrow ideas from Jaisankar et al. [7] to regulate this artificial dissipation. In particular, we blend this diffusion regulation (aptly called DR), with the Rusanov implementation of the approximate Riemann flux. Numerical experiments (both inviscid and viscous) were conducted to compare and contrast the newly formulated DR and the traditional formulations. The simulations performed with the DR showed dramatic improvements over those employing the traditional approach for 2nd, 3rd and 4th order simulations. Moreover, the DR does not interfere with the viscous flux discretization procedure. Hence it can be used in conjunction, with any viscous flux discretization procedure like the LDG [8, 11], LDG2 [10, 12], penalty [9, 11] or the BR2 [9, 11] formulations.

The paper is organized as follows. In the next section, we review the basics of the SV method. The basics of the DR are discussed in Section 3. Section 4 presents with the different test cases conducted in this study. Finally conclusions from this study are summarized in Section 5.

2 Basics of the spectral volume method

2.1 General formulation

Consider the general conservation equation

$$\frac{\partial Q}{\partial t} + \frac{\partial(f_i(Q) - f_v(Q))}{\partial x} + \frac{\partial(g_i(Q) - g_v(Q))}{\partial y} = 0, \tag{2.1}$$

in domain Ω with appropriate initial and boundary conditions. In (2.1), x and y are the Cartesian coordinates and $(x,y) \in \Omega$, $t \in [0,T]$ denotes time, Q is the vector of conserved variables, and f_i and g_i are the inviscid fluxes in the x and y directions, respectively. f_v and g_v are the viscous fluxes in the x and y directions, respectively. Domain Ω is discretized into I non-overlapping triangular (2D) cells. In the SV method, the simplex grid cells are called SVs, denoted S_i, which are further partitioned into CVs, denoted C_{ij}, which depend on the degree of the polynomial reconstruction. Fig. 1 shows linear, quadratic and cubic partitions in 1D. Fig. 2 shows the same in 2D.
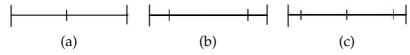

(a)　　　　　　　　(b)　　　　　　　　(c)

Figure 1: Partitions of a SV in 1D. Linear, quadratic and cubic reconstructions are shown in (a), (b) and (c) respectively.
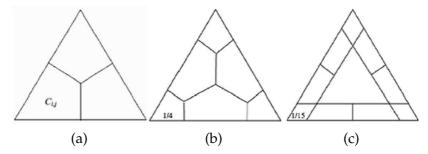

(a)　　　　　　　　(b)　　　　　　　　(c)

Figure 2: Partitions of a triangular SV. Linear, quadratic and cubic reconstructions are shown in (a), (b) and (c) respectively.

We need N unknown control volume solution averages (or DOFs) to construct a degree k polynomial. N is calculated using the below formula (in 2D)

$$N = \frac{(k+1)(k+2)}{2}, \tag{2.2}$$

where k is the degrees of the polynomial, constructed using the CV solution averages. The CV averaged conserved variable for C_{ij} is defined as

$$\overline{Q}_{i,j} = \frac{1}{V_{i,j}} \int_{C_{i,j}} Q dV, \qquad j=1,\cdots,N, \quad i=1,\cdots,I, \tag{2.3}$$

where $V_{i,j}$ is the volume of C_{ij}. Given the CV averaged conserved variables, a degree k polynomial can be constructed such that it is $(k+1)^{\text{th}}$ order approximation to Q. In other

words, we can write the polynomial as

$$p_i(x,y) = \sum_{j=1}^{N} L_j(x,y)\overline{Q}_{i,j}, \tag{2.4}$$

where the shape functions $L_j(x,y)$ satisfy

$$\frac{1}{V_{i,j}} \int_{C_{i,j}} L_n(x,y)dV = \delta_{j,n}. \tag{2.5}$$

Eq. (2.1) is integrated over the C_{ij}. This results in the following equation

$$\frac{\partial \overline{Q}}{\partial t} + \frac{1}{V_{i,j}} \sum_{r=1}^{K} \int_{A_r} (\vec{F} \cdot \vec{n})dA = 0, \tag{2.6}$$

where $\vec{F} = (f_i - f_v, g_i - g_v)$, where A_r represents the rth face of C_{ij}, $\vec{n}$ is the outward unit normal vector of A_r and K is the number of faces in C_{ij}. The surface integration on each face is done using a $(k+1)^{\text{th}}$ order accurate Gauss quadrature formula. The fluxes are discontinuous across the SV interfaces. The inviscid fluxes are handled using a numerical Riemann flux such as the Rusanov flux [22], the Roe flux [21] or AUSM flux [17]. The handling of the viscous fluxes is discussed in the next section.

2.2   Spectral volume formulation for the diffusion equation

The following diffusion equation is considered first in domain Ω with appropriate initial and boundary conditions

$$\frac{\partial u}{\partial t} - \nabla \cdot (\mu \nabla u) = 0, \tag{2.7}$$

where μ is a positive diffusion coefficient. We define an auxiliary variable

$$\vec{q} = \nabla u. \tag{2.8}$$

Eq. (2.7) then becomes

$$\frac{\partial u}{\partial t} - \nabla \cdot (\mu \vec{q}) = 0. \tag{2.9}$$

Using the Gauss-divergence theorem, we obtain

$$\overline{\overline{\vec{q}}}_{ij} V_{ij} = \sum_{r=1}^{K} \int_{A_r} u \cdot \vec{n}dA, \tag{2.10a}$$

$$\frac{d\overline{u}_{ij}}{dt} V_{ij} - \sum_{r=1}^{K} \int_{A_r} \mu \vec{q} \cdot \vec{n}dA = 0, \tag{2.10b}$$

where $\overline{\overline{q}}_{ij}$ and $\overline{u}_{ij}$ are the CV averaged gradient and solution in C_{ij}. As the solution u is cell-wise continuous, u and $\vec{q}$ at SV boundaries are replaced by numerical fluxes $\underline{\vec{q}}$ and $\underline{u}$. The above equations thus become

$$\overline{\overline{q}}_{ij}V_{ij} = \sum_{r=1}^{K} \int_{A_r} \underline{u} \cdot \vec{n} dA, \tag{2.11a}$$

$$\frac{d\overline{u}_{ij}}{dt}V_{ij} - \sum_{r=1}^{K} \int \mu \vec{q} \cdot \vec{n} dA = 0. \tag{2.11b}$$

2.2.1 Penalty approach

A symmetric approach was given by Bassi and Rebay [4], in which the numerical fluxes are defined by

$$\underline{u} = 0.5^*(u_R + u_L), \tag{2.12a}$$
$$\underline{\vec{q}} = 0.5^*(\vec{q}_R + \vec{q}_L). \tag{2.12b}$$

Analysis by Brezzi et al. [5] showed that the approach may be unstable in some situations. Kannan et al. [11] suggested the following the penalty approach to obtain the numerical fluxes:

$$\underline{u} = 0.5^*(u_R + u_L), \tag{2.13a}$$
$$\underline{\vec{q}} = 0.5^*(\vec{q}_R + \vec{q}_L) + (u_R - u_L)\vec{n}\frac{A_r}{V_{ij}}, \tag{2.13b}$$

where $\vec{q}_L$ and $\vec{q}_R$ are the left and right state solution gradients of the face (of the CV) in consideration, A_r is the area of the face (of the CV) in consideration, V_{ij} is the CV volume.

One can see a similarity between the above equation and an approximate Riemann (like Roe, Rusanov or AUSM) flux. The approximate Riemann flux is obtained by averaging the left and right state fluxes and then adding a dissipation term. This dissipation term is

1. Proportional to the jump in the solution between the right and left states.

2. Proportional to the Jacobian term/matrix or its eigen values (The Jacobian term in 1D is $\partial \tilde{f}/\partial \tilde{Q}$). For instance, in Rusanov flux, it is the maximum eigen value of the Jacobian matrix.

Eq. (2.13b) is obtained by averaging the left and right states and then penalizing it with the penalty term. This is similar to the structure of the approximate Riemann flux. The Jacobian term in this case has a dimension of 1/length. So we picked A_r/V_{ij} as an approximation to the eigen value. The penalty term has a sign which is opposite to the dissipation term. This is because the dissipation terms come on the RHS.

3 The diffusion regulation (DR) method

In this section, we first briefly describe the basics of the DR formulation and then discuss its coupling to the Rusanov flux.

3.1 Basics of the DR formulation

The actual procedure can be explained using a 1D example. Consider the below 1D inviscid system:

$$\frac{\partial Q}{\partial t} + \frac{\partial F}{\partial x} = 0, \tag{3.1}$$

where $Q = [\rho, \rho u, \rho E]^T$ and $F = [\rho u, \rho u^2 + p, \rho u E + pu]^T$. Integrating over the control volume, and applying Gauss divergence theorem,

$$V \frac{(\overline{Q}_j^{n+1} - \overline{Q}_j^n)}{\Delta t} + (\hat{F}_{j+0.5} - \hat{F}_{j-0.5}) = 0, \tag{3.2}$$

where F is the numerical flux at the interface and is given by

$$\hat{F} = \frac{(F_L + F_R)}{2} - D \tag{3.3}$$

with L and R representing the left and the right states respectively, D representing the numerical diffusion component.

As mentioned earlier, the crux of this paper is to regulate the dissipative flux D using a pre-multiplication parameter θ. This is done to ensure that the numerical flux does not get excessive dissipation. We borrow ideas from Jaisankar et al. [7] to obtain this pre-multiplication parameter θ. This parameter is a function of the Mach number jump across the interface. Obviously the maximum value of θ is unity so as to ensure that the new formulation matches the original formulation for the worst case scenario. The DR parameter is given by

$$\theta = \frac{(\Delta M^2 + \delta^2)}{2\delta} (1 - e^{-\kappa M_\alpha}), \qquad 0 \leq |\Delta M| \leq \delta, \tag{3.4a}$$

$$\theta = |\Delta M|, \qquad \delta < |\Delta M| \leq 1, \tag{3.4b}$$

$$\theta = 1, \qquad |\Delta M| > 1, \tag{3.4c}$$

where $\Delta M = M_L - M_R$, M_α is the average of the left and the right state Mach numbers, $\delta = 0.5$ and κ is set to a big number (≈ 10). The exponential term is used to reduce the numerical dissipation to zero, when the Mach numbers become small. This is done to accurately capture steady contact discontinuities. The parameter κ is needed to ensure a steep and still smooth variation of θ in the very low Mach number region. Similarly, in smooth regions, $0 < \theta \leq \delta$. This implies that the numerical dissipation is more than halved in smooth regions. More details on the above can be obtained from Jaisankar et al. [7].

3.2 Coupling with the Rusanov flux

The Rusanov scheme is simple to implement, but has relatively high levels of numerical dissipation, when compare to other flux formulations like the Roe or HLLC formulations. The dissipation term in the Rusanov's scheme is directly proportional to the local maximum eigenvalue of the Jacobian matrix and the difference between the right and left state values:

$$D = \frac{1}{2}|\lambda|_{\max}(Q_R - Q_L).$$

(3.5)

Coupling of the DR formulation, with the Rusanov flux results in

$$\hat{F} = \frac{F_L + F_R}{2} - \frac{\theta}{2}|\lambda|_{\max}(Q_R - Q_L).$$

(3.6)

4 Test results

In this section, we provide numerical examples to illustrate the capability of the DR based spectral volume formulation for solving the Euler and Navier Stokes equations in 2D. An implicit LU-SGS scheme was used for time advancement. Details on this time marching procedure can be found in [8, 11, 16].

4.1 Test case 1

In this section, we simulate an inviscid flow over a NACA-0012 airfoil at $Mach = 0.4$ and angle of attack of zero degree. The computational grid is shown in Fig. 3. The outer boundary is 20 chords away from the airfoil centre. Riemann invariants are employed as the BC at the far-field. The solution is smooth and hence the total entropy at any location should be technically a constant.
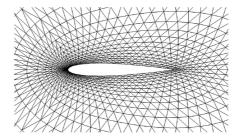

Figure 3: Grid (72∗24∗2) used for the subsonic flow over the NACA 0012.

Fig. 4 shows the second order entropy contours obtained using the two different methods. It is clear from the entropy contours that the new DR formulation produces much less spurious entropy than the traditional formulation. It must be noted that straight boundary faces were employed for these second order simulations. The third and
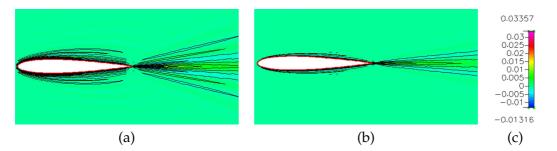
Figure 4: Entropy contours obtained for second order subsonic flow over an airfoil. Case (a): Using original formulation; Case (b): Using DR; Case (c): Legend.
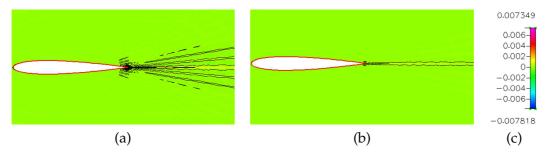

Figure 5: Entropy contours obtained for third order subsonic flow over an airfoil. Case (a): Using original formulation; Case (b): Using DR; Case (c): Legend.
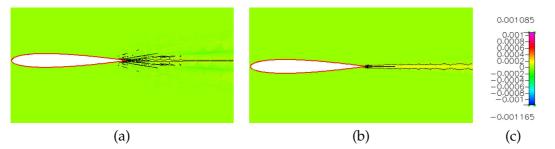

Figure 6: Entropy contours obtained for fourth order subsonic flow over an airfoil. Case (a): Using original formulation; Case (b): Using DR; Case (c): Legend.

the fourth order contours are shown in Fig. 5 and Fig. 6 respectively. The DR formulation is found to deliver higher fidelity solutions than the original formulation. Quadratic and cubic boundaries as described in [30] are adopted for the 3rd and 4th order simulations respectively.

For the sake of completeness, we also present the range of θ in Table 1. The minimum of these values is expected to monotonically decrease with increasing order. This is because, the average Mach number (average of left and right states) near the wall goes to zero, as the order increases (and as the curved wall boundary comes into effect). The upper limit is decided by the flow conditions.

Table 1: Range of θ for Test case 1.

Order	Minimum	Maximum
2	0.163	0.381
3	0.0279	0.375
4	0.00781	0.311

4.2   Test case 2

We chose a testing case of the subsonic flow over a bump at *Mach*=0.5. This case has been used by *p*-Multigrid method for DG formulations of Euler equations in [19,20] and for the SD formulations of the Euler equations by Liang et al. in [16]. A 10% thick circular bump is mounted on the centre of the channel bottom. The length of the channel is 3, its height 1, and its width 0.5. The computational grid with 3140 elements is shown in Fig. 7. The circular surface of the bump needs a higher-order boundary treatment. Quadratic and cubic boundaries as described in [30] are adopted for the 3ʳᵈ and 4ᵗʰ order simulations respectively. Riemann invariants are employed at the inlet and a fix-pressure condition is employed at the outlet.
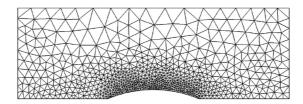

Figure 7: Grid used for the subsonic flow over a bump confined in a channel.

Based on Figs. 8-10, it is clear that the simulations obtained by the DR formulations display much smoother contours than their counterparts, which use traditional formulation. These observations are in accord with the observations made by analyzing the previous test case results.

4.3   Test case 3

This test case involves simulating the Couette flow. The Couette flow is an analytical solution of the Navier-Stokes equations, and was selected to study the accuracy for the 2D Navier-Stokes solver, using both the DR and the original formulations. This problem models the viscous flow between a stationary, fixed temperature, (at T_0) bottom plate, and a moving, fixed temperature (at T_1) top plate at speed of U. The distance between the two plates is H. Cyclic boundary conditions are employed at the inlet and the outlet.

It has an exact solution under the simplification that the viscosity coefficient μ is a constant and the speed is low enough to ensure nearly incompressible effects. The steady
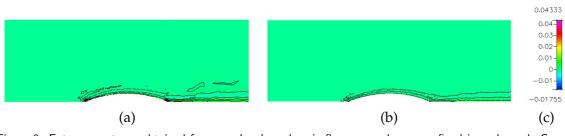
Figure 8: Entropy contours obtained for second order subsonic flow over a bump confined in a channel. Case (a): Using original formulation; Case (b): Using DR; Case (c): Legend.

Figure 9: Entropy contours obtained for third order subsonic flow over a bump confined in a channel. Case (a): Using original formulation; Case (b): Using DR; Case (c): Legend.
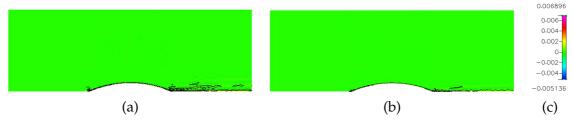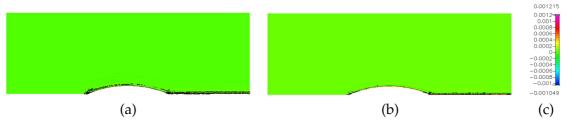

Figure 10: Entropy contours obtained for fourth order subsonic flow over a bump confined in a channel. Case (a): Using original formulation; Case (b): Using DR; Case (c): Legend.

analytic solution is

$$u = \frac{U}{H}y, \qquad v = 0, \tag{4.1a}$$

$$T = T_0 + \frac{y}{H}(T_1 - T_0) + \frac{\mu u^2}{2\kappa}\frac{y}{H}\left(1 - \frac{y}{H}\right), \tag{4.1b}$$

$$p = \text{constant}, \qquad \rho = \frac{p}{RT}, \tag{4.1c}$$

where κ is the thermal conductivity and R is the gas constant.

The accuracy of the two formulations was tested. A penalty formulation was used to discretize the viscous fluxes [9, 11]. The L_1 and the L_∞ temperature errors are presented in Table 2, Table 3 and Table 4 for 2nd, 3rd and 4th orders respectively. It can be seen that the obtained orders are very close to the ones expected. It can also be seen that the DR formulation always yields better results than the original formulation.

Table 2: Temperature error for the second order Couette flow problem.

Grid	Formulation	L_1 Error	L_1 Order	L_∞ Error	L_∞ Order
10×10×2	Original	5.976e-05	-	2.115e-04	-
10×10×2	DR	5.911e-05	-	2.074e-04	-
20×20×2	Original	1.500e-05	1.99	5.197e-05	2.03
20×20×2	DR	1.427e-05	2.05	4.952e-05	2.07
40×40×2	Original	3.743e-06	2.00	1.335e-05	1.96
40×40×2	DR	3.482e-06	2.03	1.151e-05	2.10

Table 3: Temperature error for the third order Couette flow problem.

Grid	Formulation	L_1 Error	L_1 Order	L_∞ Error	L_∞ Order
10×10×2	Original	1.043e-07	-	3.546e-07	-
10×10×2	DR	6.842e-08	-	2.681e-07	-
20×20×2	Original	1.278e-08	3.03	3.769e-08	3.23
20×20×2	DR	8.672e-09	2.98	3.052e-08	3.14
40×40×2	Original	1.599e-09	3.00	4.824e-09	2.97
40×40×2	DR	1.130e-09	2.94	3.923e-09	2.96

Table 4: Temperature error for the fourth order Couette flow problem.

Grid	Formulation	L_1 Error	L_1 Order	L_∞ Error	L_∞ Order
10×10×2	Original	1.247e-08	-	2.728e-08	-
10×10×2	DR	1.051e-08	-	2.263e-08	-
20×20×2	Original	7.648e-10	4.03	1.775e-09	3.94
20×20×2	DR	6.523e-10	4.01	1.444e-09	3.97

4.4 Test case 4

In this section, we simulate flow over a NACA 0012 airfoil. The flow was subsonic at *Mach* = 0.5 and had a zero angle of attack. The Reynolds number was 5000. This has been a widely used validation case for viscous flow solvers and was used in [11–13]. The computational grid is the same as the one used in the first test case. An important trait of this test case is the formation of a small recirculation bubble that extends in the near wake region of the airfoil. This is caused due to the separation of the flow near the trailing edge. A penalty formulation was used to discretize the viscous fluxes [9,11].

The current simulations were performed using the two formulations for 2nd, 3rd and 4th orders. These are compared with the ones performed in [11–13]. These comparisons are summarized in Table 5. It is reasonable to assume that the 5th order spectral difference results of Sun et al. [23] are the most accurate of all the ones listed in Table 5. This table compares the separation point, drag coefficient due to pressure (CD_p) and the drag coefficient due to viscous stresses (CD_f).

It can be seen that the DR simulations consistently outperform their traditional coun-

Table 5: Comparison of pressure and viscous drag coefficients and location of separation point in a flow over an airfoil simulation, using DR and the original formulations.

Method	NDOFs	Separation Point	(CD_p)	(CD_f)
2nd order SV (Original)	10368	94.2%	2.0498e-2	3.5570e-2
2nd order SV (DR)	10368	91.9%	2.1610e-2	3.3970e-2
3rd order SV (Original)	20736	81.7%	2.2081e-2	3.2206e-2
3rd order SV (DR)	20736	81.6%	2.2114e-2	3.2397e-2
4th order SV (Original)	34560	81.3%	2.2270e-2	3.2374e-2
4th order SV (DR)	34560	81.3%	2.2267e-2	3.2405e-2
5th order SD [23]	43200	81.4%	2.2250e-2	3.2510e-2

terparts for the 2nd, 3rd and 4th order simulations. The above two test cases, demonstrate that this DR formulation works equally well for the Navier-Stokes equations as well.

Fig. 11 shows the Mach contours computed with linear and quadratic SVs using the DR formulation. The solution gets smoother and smoother with the increasing of the order of the polynomial reconstruction. The wake region looks more refined and continuous for the 3rd order case. The difference between the 3rd and the 4th order plots were negligible. The Mach contours computed using the traditional formulation look visually similar and hence are not shown in this paper.
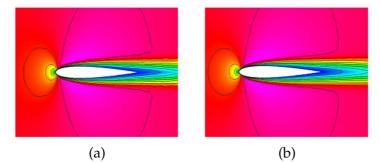

(a)   (b)

Figure 11: Mach contours around the NACA0012 airfoil at zero degree of attack, $Re=1000$, $M=0.5$. Case (a): 2nd order; Case (b): 3rd order.

5 Conclusions

The diffusion regulation (DR) approach, postulated by Jaisankar et al. [7] was implemented in the high order spectral volume context. This approach modifies the jump in the Rusanov flux, based on the jump in the Mach number. This modification in the Rusanov flux jump is locally decided, automatic and needs no user intervention. The numerical test cases indicated that this formulation was able to improve the fidelity of the high order spectral volume method for both Euler and Navier Stokes equations and for all the orders.

Future work will involve coupling of this DR formulation to other approximate Riemann fluxes like the Roe and the HLLC fluxes, applications to discontinuous regimes and cases involving highly skewed meshes. The final goal of this project would be to extend this formulation to more complex 3D flows, such as turbulent combustion, explosions, and multiphase flows, as undertaken by Balakrishnan and co-workers [1–3]. Such problems also involve hydrodynamic instabilities, whose growth rates cannot be captured accurately when used in conjunction with the traditional second order low dissipation Rusanov flux.

Acknowledgments

References

[1] K. Balakrishnan and S. Menon, On the role of ambient reactive particles in the mixing and afterburn behind explosive blast waves, Combust. Sci. Technol., 182(2) (2010), 186–214.
[2] K. Balakrishnan and S. Menon, On turbulent chemical explosions into dilute aluminium particle clouds, Combust. Theor. Model., 14(4) (2010), 583–617.
[3] K. Balakrishnan, D. V. Nance and S. Menon, Simulation of impulse effects from explosive charges containing metal particles, Shock Waves, 20(3) (2010), 217–239.
[4] F. Bassi and S. Rebay, A high-order accurate discontinuous finite element method for the numerical solution of the compressible Navier Stokes equations, J. Comput. Phys., 131 (1997), 267–279.
[5] F. Brezzi, G. Manzini, D. Marini, P. Pietra and A. Russo, Discontinuous Galerkin approximations for elliptic problems, Numer. Methods Partial Differ. Equations, 16 (2000), 365–378.
[6] B. Cockburn and C.-W. Shu, The local discontinuous Galerkin method for time-dependent convection diffusion system, SIAM J. Numer. Anal., 35 (1998), 2440–2463.
[7] S. Jaisankar and S. V. Raghurama Rao, Diffusion regulation for Euler solvers, J. Comput. Phys., 221 (2007), 577–599.
[8] R. Kannan, High order spectral volume method for moment models in semiconductor device simulations: formulation in 1D and application to a p-multigrid method, Int. J. Numer. Methods Biom. Eng., 27(9) (2011), 1362–1375.
[9] R. Kannan, High order spectral volume method for moment models in semiconductor device simulations II: Accuracy studies and performance enhancements using the penalty and the BR2 formulations, Int. J. Numer. Methods Biom. Eng., 27(5) (2011), 650-665.
[10] R. Kannan, An implicit LU-SGS spectral volume method for the moment models in device simulations III: accuracy enhancement using the LDG2 flux formulation for non-uniform grids, Int. J. Numer. Model. El., accepted.
[11] R. Kannan and Z. J. Wang, A study of viscous flux formulations for a p-multigrid spectral volume Navier stokes solver, J. Sci. Comput., 41(2) 2009, 165–199.
[12] R. Kannan and Z. J. Wang, LDG2: a variant of the LDG viscous flux formulation for the spectral volume method, J. Sci. Comput., 46(2) (2011), 314–328.

[13] R. Kannan and Z. J. Wang, The direct discontinuous Galerkin (DDG) viscous flux scheme for the high order spectral volume method, Comput. Fluids, 39(10) (2010), 2007–2021.

[14] R. Kannan and Z. J. Wang, Curvature and entropy based wall boundary condition for the high order spectral volume Euler solver, Comput. Fluids, 44(1) (2011), 79–88.

[15] R. Kannan, A high order spectral volume method for elastohydrodynamic lubrication problems: formulation and application of an implicit p-multigrid algorithm for line contact problems, Comput. Fluids, 48(1) (2011), 44–53.

[16] C. Liang, R. Kannan and Z. J. Wang, A p-multigrid spectral difference method with explicit and implicit smoothers on unstructured grids, Comput. Fluids, 38(2) (2009), 254–265.

[17] M.-S. Liou and C. Steffen, A new flux splitting scheme, J. Comput. Phys., 107 (1993), 23–39.

[18] Y. Liu, M. Vinokur and Z. J. Wang, Spectral (finite) volume method for conservation laws on unstructured grids V: extension to three-dimensional systems, J. Comput. Phys., 212 (2006), 454–472.

[19] H. Luo, J. D. Baum and R. Löhner, A p-multigrid discontinuous Galerkin method for the Euler equations on unstructured grids, J. Comput. Phys., 211 (2006), 767–783.

[20] C. R. Nastase and D. J. Mavriplis, High-order discontinuous Galerkin methods using an hp-multigrid approach, J. Comput. Phys., 213 (2006), 330–357.

[21] P. L. Roe, Approximate Riemann solvers, parameter vectors and difference schemes, J. Comput. Phys., 43 (1981), 357–372.

[22] V. V. Rusanov, Calculation of interaction of non-steady shock waves with obstacles, J. Comput. Math. Phys., USSR 1 (1961), 267–279.

[23] Y. Sun and Z. J. Wang, Efficient implicit non-linear LU-SGS approach for compressible flow computation using high-order spectral difference method, Commun. Comput. Phys., submitted.

[24] Y. Sun, Z. J. Wang and Y. Liu, Spectral (finite) volume method for conservation laws on unstructured grids VI: extension to viscous flow, J. Comput. Phys., 215 (2006), 41–58.

[25] C-W. Shu, Total-variation-diminishing time discretizations, SIAM J. Sci. Stat. Comput., 9 (1988), 1073–1084.

[26] Z. J. Wang, Spectral (finite) volume method for conservation laws on unstructured grids: basic formulation, J. Comput. Phys., 178 (2002), 210.

[27] Z. J. Wang and Y. Liu, Spectral (finite) volume method for conservation laws on unstructured grids II: extension to two-dimensional scalar equation, J. Comput. Phys., 179 (2002), 665.

[28] Z. J. Wang and Y. Liu, Spectral (finite) volume method for conservation laws on unstructured grids III: extension to one-dimensional systems, J. Sci. Comput., 20 (2004), 137.

[29] Z. J. Wang and Y. Liu, Spectral (finite) volume method for conservation laws on unstructured grids IV: extension to two-dimensional Euler equations, J. Comput. Phys., 194 (2004), 716.

[30] Z. J. Wang and Y. Liu, Extension of the spectral volume method to high-order boundary representation, J. Comput. Phys., 211 (2006), 154–178.